Microscopy AND
Microanalysis

Melamine–Formaldehyde Microcapsules: Micro- and Nanostructural Characterization with Electron Microscopy

Hamed Heidari,[1,*,†] Guadalupe Rivero,[2,3,†] Hosni Idrissi,[1,4] Dhanya Ramachandran,[1] Seda Cakir,[2] Ricardo Egoavil,[1] Mert Kurttepeli,[1] Amandine C. Crabbé,[5] Tom Hauffman,[5] Herman Terryn,[5] Filip Du Prez,[2] and Dominique Schryvers[1]

[1]*Electron Microscopy for Materials Science (EMAT), University of Antwerp, Groenenborgerlaan 171, 2020 Antwerp, Belgium*
[2]*Department of Organic and Macromolecular Chemistry, Polymer Chemistry Research Group, Ghent University, Krijgslaan 281 S4, 9000 Ghent, Belgium*
[3]*Instituto de Investigaciones en Ciencia y Tecnología de Materiales (INTEMA) J.B, Justo 4302, B7608FDQ Mar del Plata, Argentina*
[4]*Institute of Mechanics, Materials and Civil Engineering, Université catholique de Louvain, Place Sainte Barbe 2, B-1348 Louvain-la-Neuve, Belgium*
[5]*Research Group Electrochemical and Surface Engineering (SURF), Department of Materials and Chemistry, Vrije Universiteit Brussel, Pleinlaan 2, 1050 Brussels, Belgium*

Abstract: A systematic study has been carried out to compare the surface morphology, shell thickness, mechanical properties, and binding behavior of melamine–formaldehyde microcapsules of 5–30 μm diameter size with various amounts of core content by using scanning and transmission electron microscopy including electron tomography, *in situ* nanomechanical tensile testing, and electron energy-loss spectroscopy. It is found that porosities are present on the outside surface of the capsule shell, but not on the inner surface of the shell. Nanomechanical tensile tests on the capsule shells reveal that Young's modulus of the shell material is higher than that of bulk melamine–formaldehyde and that the shells exhibit a larger fracture strain compared with the bulk. Core-loss elemental analysis of microcapsules embedded in epoxy indicates that during the curing process, the microcapsule-matrix interface remains uniform and the epoxy matrix penetrates into the surface micro-porosities of the capsule shells.

Key words: transmission electron microscopy, melamine formaldehyde, in situ mechanical TEM, electron tomography, EELS

INTRODUCTION

Microcapsules (Yow & Routh, 2006) (MCs) have gained increasing importance as they can isolate active core ingredients surrounded by a polymer shell, providing enhanced performance, stability, efficiency, or safety, depending on the desired application. Encapsulation technologies (Andrade et al., 2015) find applications in the development of self-healing composite materials (Hillewaere et al., 2014; Hillewaere & Du Prez, 2015), drug delivery vesicles (Devarajan & Jain, 2014), triggered catalytic systems (Deleu et al., 2015), smart textiles (Nelson, 2002), food technology (Shahidi & Han, 1993), cosmetics, etc. In case of self-healing composites, MCs are usually embedded in a polymeric matrix and are expected to break when hit by a crack. As such, reactive core ingredients are released forming a polymer and immediately closing the crack. Information on the microstructure as well as mechanical strength of the shell is thus crucial in understanding the properties and behavior of such composite materials and improving their potential applications.

Theoretically, factors influencing the mechanical strength of MCs are their chemical structure, composition, surface morphology, shell thickness, and the overall size of the MC. By controlling these factors, it is possible to tune the properties of the capsules to effectively break the shell at the crack in order to release the core contents.

Mechanical behavior of melamine–formaldehyde (MF) MCs studied using micromanipulation, atomic force microscopy, compression, and nano-indentation techniques has been reported (Sun & Zhang, 2001; Hu et al., 2009; Pretzl et al., 2012; Su et al., 2012; Long et al., 2013; Neubauer et al., 2014). However, no reports have been published demonstrating the use of *in situ* transmission electron microscopy (TEM) tensile testing on the MC shells as well as on advanced TEM techniques used to characterize the intrinsic MC properties. Furthermore, for the MCs to exhibit good self-healing ability, it is important to understand their interaction with the matrix. Delamination triggered by poor adhesion among the MC shell and the surrounding matrix could deviate the crack, so that it propagates around the MC. In this work we focus on the electron microscopy characterization of intrinsic properties of MF MCs containing cyclohexane, and their binding behavior within

an epoxy matrix. MCs with two different core contents were investigated, as-prepared and after core extraction.

MATERIALS AND METHODS

Synthesis and Purification

Melamine was purchased from Aldrich (St. Louis, Missouri, USA). Formaldehyde solution (37%), triethanolamine, cyclohexane, polystyrene alt maleic anhydride, partial methyl ester (Mn:350000) (PSMA), magnesium chloride hexahydrate, and 1-octanol were purchased from Sigma-Aldrich (St. Louis, Missouri, USA). Sulfuric acid (95–97%) was available from Chemlab (Pittsburgh, Pennsylvania, USA). All materials were used without further purification.

For preparation of the epoxy matrix, bisphenol A diglycidyl ether (BADGE, molecular weight (MW) = 340.4 g/mol) and isophorone diamine (5-amino-1,3,3-trimethyl cyclohexane, MW = 170.3 g/mol) were used from Sigma-Aldrich. Jeffamine D-400 (polyoxyalkyleneamine, MW = 430 g/mol) from Huntsman, whereas 1,6-hexanediol diglycidyl ether (Heloxy modifier HD, MW = 230.3 g/mol) was provided by Momentive (Columbus, Ohio, USA).

Preparation of MCs

The procedure was adapted from (Yuan et al., 2008). The pre-condensate pre-polymer was prepared by mixing 12 g of melamine and 25 mL of formaldehyde solution (37%). The pH was adjusted to 9 by adding triethanolamine. The mixture was heated in an oil bath at 70°C for 30 min until it became transparent. In parallel, the emulsion was prepared by mixing cyclohexane with 200 mL of 2% aqueous solution of PSMA. MCs with two different amounts of core content were prepared. In one case, 60 g of cyclohexane was used for the type MC1 capsules, whereas half of this amount (30 g) was encapsulated in the type MC2 capsules. The pH was slowly decreased to 5 by dropwise addition of sulfuric acid solution (13%), whereas the mixture was homogenized at a speed of 7,000 rpm with an UltraTurrax (IKA) device (IKA®-Werke GmbH & Co., Staufen, Germany). One or two drops of 1-octanol were added in order to control the foam. Maintaining pH at 5 is a critical step to control the agglomeration or material precipitation. Finally, the stable emulsion was transferred to a reactor with mechanical agitation with a four-bladed stirrer at 400 rpm. A quantity of 200 mL of water was added at this stage. The pre-reacted pre-polymer was slowly added to the reactor, leading to a sharp pH increase that was controlled by the addition of sulfuric acid (13%) solution, during the incorporation. After completing the addition of the pre-condensate, 10.65 g of magnesium chloride hexahydrate (dissolved in 20 mL of water) was slowly added to the reactor. The final pH was adjusted to 5. The reactor was heated from room temperature to 50°C and the MC slurry was collected after 1 h. MCs were kept in the slurry form until usage. For characterization, MCs were filtered with filter paper, washed with water, and dried in a vacuum oven at 40°C overnight.

Embedding of MCs

The epoxy matrix was prepared by using an amine hardener mixture of Jeffamine D-400/isophorone diamine with a molecular ratio of 50/50 and an epoxy mixture of BADGE/1,6-hexanediol diglycidyl ether with a molar ratio of 92/8. The amine mixture was mixed with the epoxy mixture with a weight ratio of 26/74. Finally, it was cured with a 10 wt% MC loading for 24 h at 40°C and 24 h at 80°C in the oven.

Characterization of MCs

The core content was determined by Soxhlet extraction. A precise amount of dried MCs was placed in a cellulose thimble located in the main chamber of the Soxhlet extractor and connected to a reflux condenser and a distillation flask filled with acetone. The flask was heated to reflux at 70°C for 48 h. Solid shells recovered from the thimble were dried in a vacuum oven and weighted. Core content was calculated as $(1 - \text{shell fraction}) \times 100$. After extraction, the resulting empty capsules of each type (named MC1X and MC2X) were further analyzed and differences in their structure/surface morphology were investigated.

Scanning Electron Microscopy (SEM)

The surface morphology and shell thickness of the MCs was examined using a FEI Quanta FEG 250 SEM operating at 10 kV. For this purpose, MCs were mounted on a conductive stage and coated with a 20 nm layer of carbon to diminish charging. The capsules were then ruptured using a sharp blade to study the morphology and thickness of the shell wall.

Electron Tomography

For electron tomography, thin cross-sections were prepared by focused ion beam (FIB) milling using a FEI Nova 200 FIB/SEM dual beam system (FEI Company, part of Thermo Fisher Scientific, Hillsboro, Oregon, USA). The procedure can be followed in Figure 1. Before milling, a Pt layer was deposited on top of the surface of the MC shell, seen as an even bright layer in Figure 1b. Next, an undercut was carried out using a beam current of 230 pA on either sides of the region of interest to obtain a strip with a thickness of 200 nm. Subsequently, the strip was transferred to a 3 mm TEM Cu grid using an Omniprobe micromanipulator (Oxford Instruments PLC, Tubney Woods, Abingdon, Oxfordshire, UK), seen in Figures 1c and 1d. After attachment of the sample using Pt deposition, the Omniprobe was detached from the strip.

Electron tomography acquisition was performed on such strips. Tomography tilt series were recorded using a FEI Osiris TEM (FEI Company) operated at 200 kV in scanning transmission electron microscopy (STEM) mode. A dedicated single tilt tomography holder (Fischione model 2020) was used to acquire high angle annular dark field (HAADF) STEM images with a tilt increment of 2° over a tilt range of ±74°. Alignment of the recorded images was carried out in the FEI Inspect3D tomography package (FEI Company).
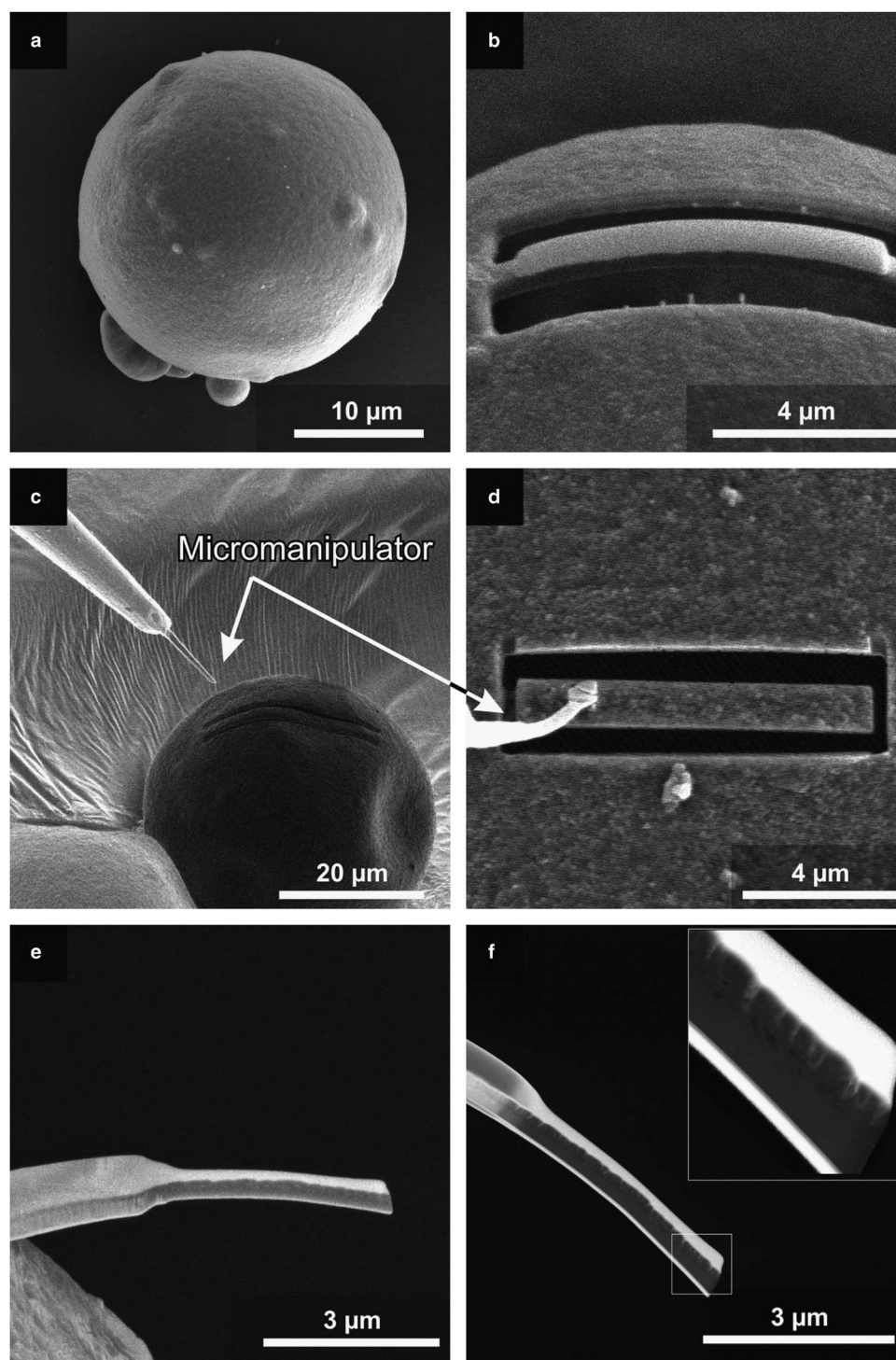
Figure 1. Preparation of a strip sample for electron tomography using FIB from the microcapsule shell. **a**: SEM view of MC1. **b**: After deposition of a protecting Pt layer on top of the region of interest, trenches were cut around the strip using FIB. **c,d**: Strip is lifted-out using a micromanipulator. **e**: SEM image of the final sample attached to a TEM grid. **f**: Nano-pores visible at the side of the strip in a transmitted HAADF-STEM image.

Tomographic reconstructions were obtained using the "Simultaneous Iterative Reconstruction Technique" with 50 iterations implemented in the ASTRA tomography toolbox (van Aarle et al., 2015). Amira (FEI Software) was used for visualization of the reconstructed volumes. Volume rendering visualization videos of the three-dimensional

(3D) reconstructions are provided in the supporting information.

In Situ TEM Nano Tensile Test
In situ TEM uniaxial tensile experiments were performed on sub-micron strips cut from the capsule shells. Experiments
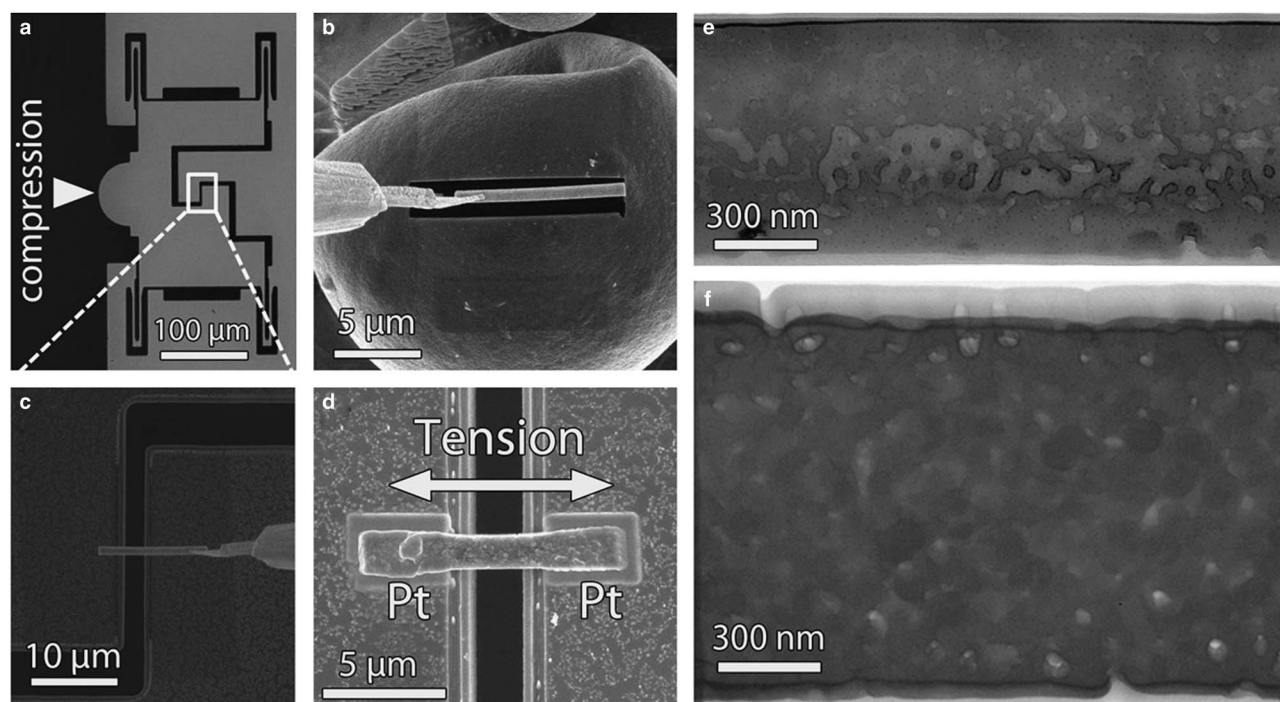
Figure 2. a: Optical micrograph of the PTP device used for in-situ TEM tensile experiments. The compression of the semi-circular end in (**a**) induces uniaxial tension in the middle gap shown in (**c**) and (**d**). **b**: FIB cutting and extraction of a tensile sample from the microcapsule (**c**) SEM images showing the transfer of the sample onto the PTP device. **d**: Mounting of the sample in the middle gap of the PTP using electron beam deposited Pt. **e** and **f**: BF-TEM micrographs obtained on tensile samples prepared from the microcapsules MC1 and MC2, respectively.

were accomplished in load controlled mode using a conductive diamond flat punch indenter in the PI 95 TEM PicoIndenter from Hysitron Inc (Eden Praire, Minnesota, USA). A special micro-electro-mechanical-system device called push-to-pull (PTP) was used (Fig. 2a). Owing to four identical springs distributed symmetrically at the corners of this device, the compression (push) of the semi-circular end of the PTP device using the flat punch indenter is converted into a uniaxial tensile loading (pull) on the middle gap of the PTP device (Fig. 2a). The springs are arranged in such a way that the force acting on them is parallel to the force on the tensile specimen. The transducer of the PI 95 TEM PicoIndenter (Hysitron Inc.) exhibits load and displacement resolution below 3 nN and 0.02 nm, respectively. The load and displacement noise floor are around 200 nN and 0.4 nm, respectively. The raw force was obtained as a combination of the force applied on the sample and the PTP device. The spring constant of the PTP device was extracted by performing *in situ* TEM tensile tests on the empty PTP device after the fracture of the samples and found to be 15 N/m. The force on the sample was thus extracted by subtracting the contribution of the PTP device from the raw force. The engineering stress was obtained by dividing the force on the sample by the cross-sectional area measured on SEM images, whereas the engineering strain was calculated by dividing the raw displacement data by the initial gage length measured on the plan-view SEM images. The raw displacement was measured frame-by-frame on the recorded TEM

videos using digital image correlation. The reliability of the acquired data was verified according to Idrissi et al. (2014, 2016).

Two tensile samples were cut from capsules MC1 and MC2, respectively (Fig. 2b) and transferred to the PTP device using the Omniprobe micromanipulator (Fig. 2c). The samples were then attached to the PTP device using electron beam deposited Pt (Fig. 2d). In order to avoid Ga+ ion beam damage to the gage section during transfer of the tensile samples to the PTP device, the samples were only locally exposed to the ion beam, outside the gage sections used for the tensile tests. A tensile sample of $4.38\,\mu m$ length, 757 nm width, and 476.0 nm thickness (MC1) and one of $3.53\,\mu m$ length, $1.29\,\mu m$ width, and 622.7 nm thickness (MC2) were prepared using FIB. The initial microstructure of these samples can be seen in the bright-field TEM images of Figures 2e and 2f, respectively.

The *in situ* tensile tests were run in a FEI-Osiris microscope operating at 200 kV and equipped with a high brightness XFEG (Field Emission Gun) source. The experiments were performed with a loading rate of $1\,\mu N/s$. The instrument is fully remote controlled from an operator room outside the room of the microscope leading to a higher stability during the *in situ* TEM nanomechanical testing experiments. Video sequences were recorded by a Gatan Ultrascan CCD camera (Gatan, Inc., Pleasanton, CA, USA) with a post-specimen shutter and a spatial resolution of 2×2 K at a frame rate of 5 fps.

Electron Energy-Loss Spectroscopy (EELS)

In order to investigate the embedded MCs in epoxy matrix, ultra-thin sections were prepared using a Leica EM UC7-ultramicrotome (Leica - microsystems Vertrieb GmbH, Wetzlar, Germany) with a thickness of ~30 nm. The ultra-thin sections were then transferred to a 3 mm TEM copper grid. In order to increase the stability of the films under the electron beam, a thin layer of 3–5 nm amorphous carbon was deposited on the sections. EELS was performed using a FEI Titan TEM (FEI Company) operated at 300 kV in STEM mode. An energy resolution of 1.0 eV, determined from the full-width-at-half-maximum of the zero energy-loss peak was obtained for the EELS measurements. The STEM convergence and collection semi-angles used were 21 and 175 mrad, respectively. The quantitative elemental profiles were obtained by subtracting a power-law background and a subsequent integration of the corresponding core-loss excitation edge for each element. Analyses of the EELS spectra were performed using Gatan Digital Micrograph.

Raman Spectroscopy

The Raman spectroscopy measurements were performed using a DILOR XY spectrometer (HORIBA Jobin Yvon Inc., NJ, USA) equipped with an Olympus (Olypus, Tokyo, Japan) BH2 microscope (magnification 50×, long focal length of 8 mm), a single monochromater, an edge filter and liquid-nitrogen-cooled charge-coupled device detector CCD 3000 with a resolution of ~2 cm^{-1}. Samples were excited with 514 nm radiation of a Coherent Innova 70C Ar/Kr mixed gas laser (Coherent Inc., Santa Clara, CA, USA).

The chemical composition and distribution of the sample were determined by using reference materials. Characteristic Raman peaks were determined for each of the constituting materials of the MCs (at 802 cm^{-1} for the cyclohexane and 1,111 cm^{-1} for the MF). These reference peaks are present in a single frame with a 600 cm^{-1} width. Mappings were obtained using spectra taken every 1 μm. The spectra and mappings were treated with LabSpec (Dilor) software.

RESULTS AND DISCUSSION

MCs containing 87 wt% (MC1) and 62 wt% (MC2) of cyclohexane were prepared and characterized. The core content of

each sample type was extracted and the resulting empty capsules (MC1X and MC2X) were further characterized. Differences in the amount of core material affected the shell thickness of the resulting MCs. Lower amounts of added core material, as in MC2, yield a smaller total surface area, which yields thicker shells when covered by a fixed amount of pre-polymer. MCs with similar sizes (20–30 μm, which is around the average value for capsule diameter in these distributions) were selected for further investigation in the original and extracted forms. Table 1 indicates the labels and specifications of each investigated MC to facilitate the tracking of samples.

Figures 3a—3d show SEM micrographs of both MC types, showing that the polydisperse MF MCs were spherical in shape with a wrinkle free surface morphology. Regardless of the size, they all exhibit similar shell thicknesses, as shown in Supplementary Fig. S2. A closer look at the outside surface morphology of the MCs shows a smooth surface but with granular features (Figs. 3b, 3d) in the range of 100–160 nm. Also, the roughness of the surface of MC2 is stronger compared with MC1. The granular MF particles, adhered to the surface, might be a result of the competition between the separation/solidification of the shell and the formation of individual precursor particles in the aqueous phase that can further coalesce and deposit in the surface (Jahromi et al., 1999; Yuan et al., 2008; Blaiszik et al., 2009). Again, given that the same amount of shell-forming pre-polymer was used for both capsule types, but less core was available in MC2, it is possible that once the shell is formed in the latter case, the rest of the pre-polymer remains in the medium as particles and eventually deposits on the surface yielding a rougher outside layer. In contrast, when there are more core droplets to be "coated" as in MC1, the pre-polymer is preferentially used for proper shell formation, an evidence for this hypothesis is given in Supplementary Figures S2(e) and S2(f), where a cross-section image of the embedded MCs is shown.

Supplementary Figures S2(e) and S2(f)

Supplementary Figures S2(e) and S2(f) can be found online. Please visit journals.cambridge.org/jid_MAM.

SEM images of the broken capsule shells are shown in Figure 3e (MC1) and Figure 3f (MC2). Various microcracks were observed, propagating through the apparently brittle shell of the MCs. The chemical composition of the MCs shell and core material was characterized with Raman spectroscopy. Figure 4 presents a Raman spectral mapping of an MC2, freshly dried from a water-based slurry. The concentration of the core material is evaluated by comparing the intensity of the cyclohexane peak at 802 cm^{-1} (left window) with the one of the shell material using the MF peak present at 1,111 cm^{-1} (right window).

It can be seen from Figure 4 that cyclohexane is present in the core of the MC after drying. However, the cyclohexane
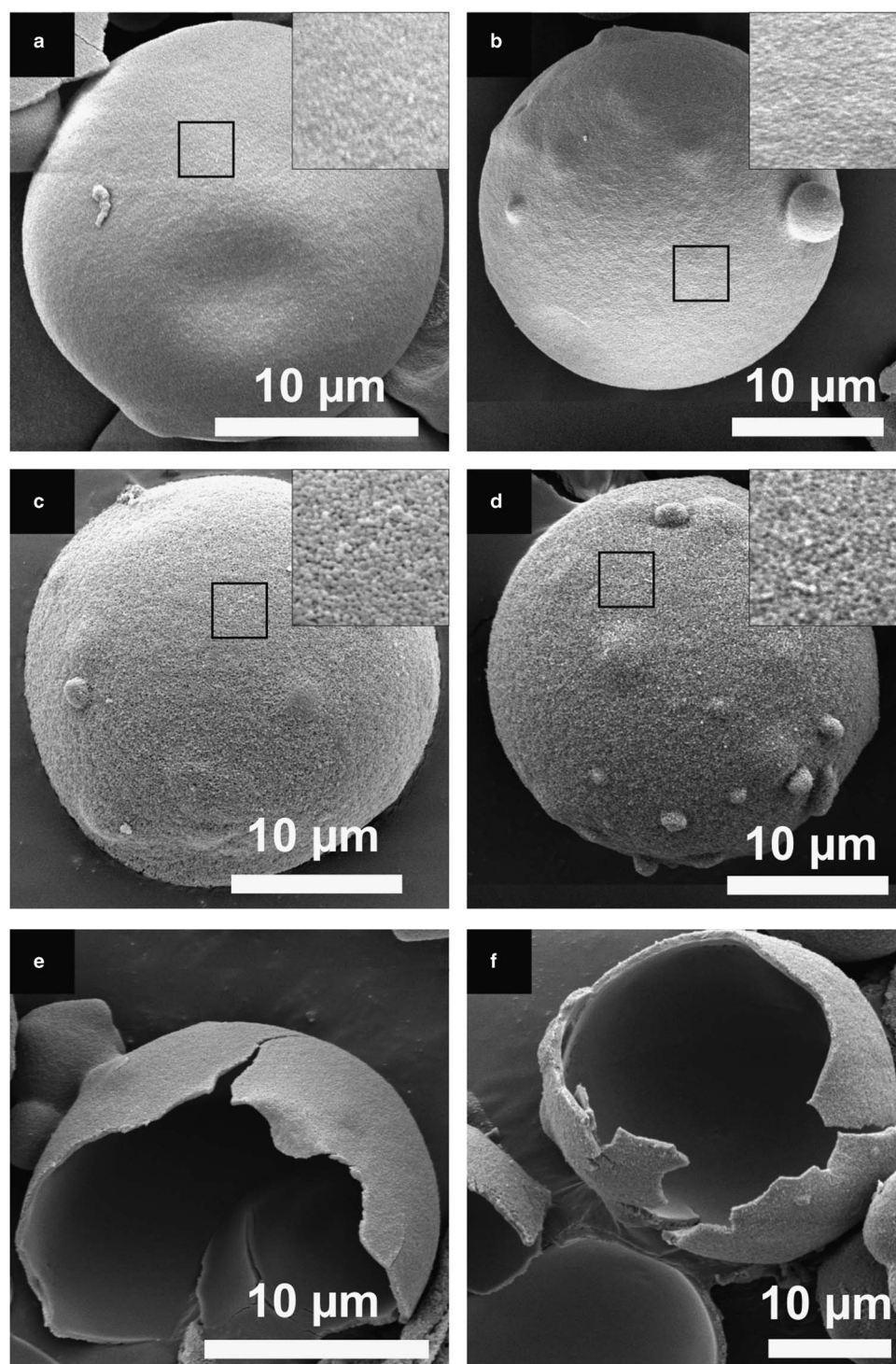
Table 1. Labeling and Specifications of the Investigated Microcapsules.

Sample Label	Percent of Cyclohexane Core Content (wt%)	Extracted Core	Shell Thickness (From SEM Measurements) (nm)
MC1X	—	Yes	580–800
MC1	86.9	No	550–700
MC2X	—	Yes	890–1,300
MC2	61.7	No	900–1,240

Figure 3. SEM images of the microcapsules. **a,b**: Overview of MC1X and MC1, respectively. **c,d**: Overview of MC2X and MC2, respectively. Insets indicate the surface roughness of the microcapsules. **e,f**: Ruptured shell of the MC1 and MC2, respectively, exhibiting the brittle nature of the shells.

signal is also present in the shell and even outside the MC. In order to elucidate the possible origin of the cyclohexane inside the shell, the internal structure of the shell was examined in more detail. Therefore, cross-section samples from the shell prepared by FIB were investigated. Figure 5 shows the presence of micro-channels over the entire shell in case of MC1X. These channels are extended perpendicular to the inner and outer shell surfaces. These micro-channels have a maximum inner diameter of 90 nm (Fig. 5b, solid lines) and outer diameter of 210 nm (Fig. 5b, dashed lines), in rough agreement with the granular features found at the surface (cf. Fig. 3).
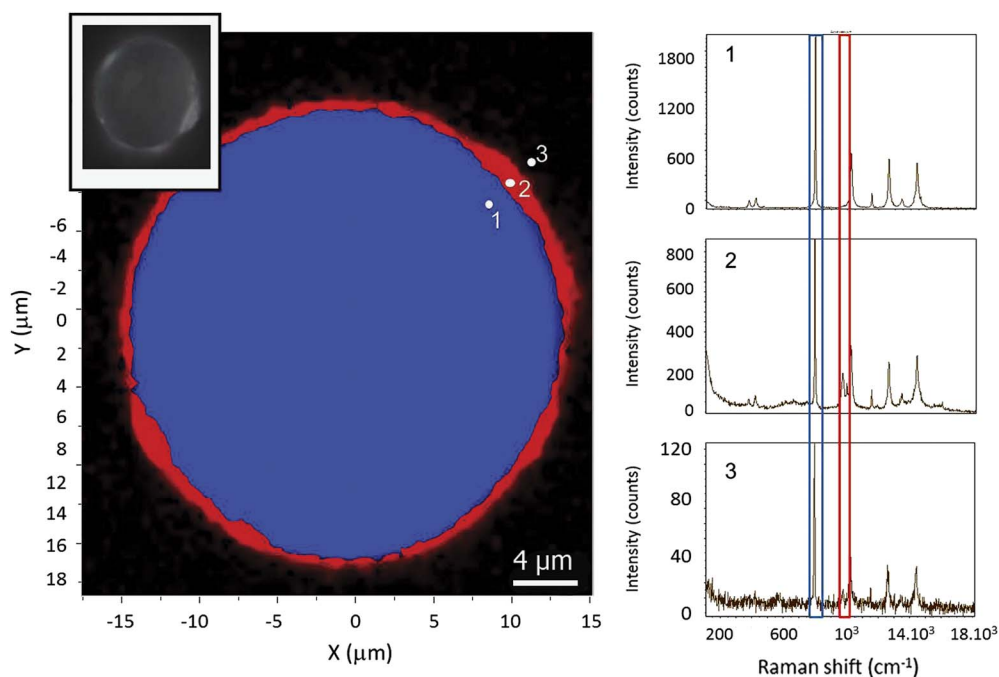
Figure 4. Raman mapping of a microcapsule (MC2) showing the distribution of the shell and the core material. The top left inset shows an optical microscope image of the analysed MC. Snapshot spectra are presented on the left to show the presence of melamine formaldehyde in the three measured positions (1: inside the capsule; 2: at the shell; 3: outside the capsule).
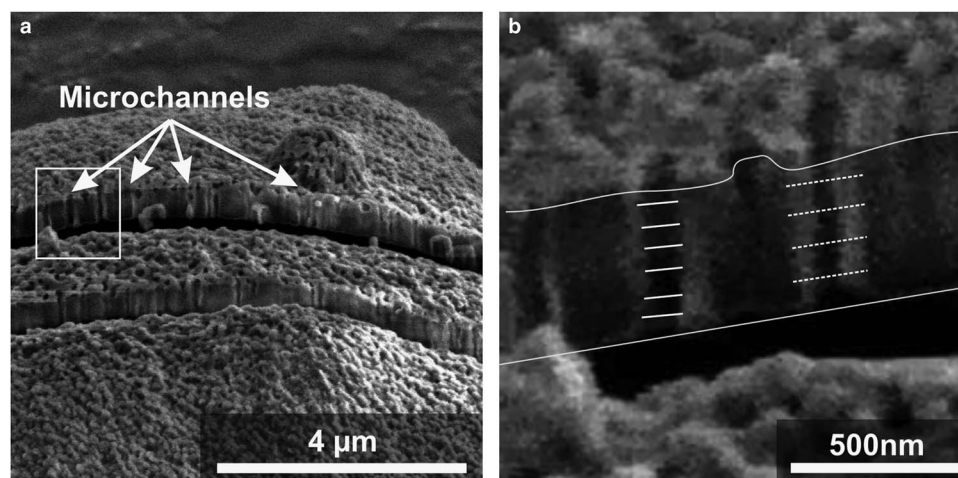

Figure 5. **a**: SEM of the FIB-milled surface of the capsule MC2X (core-extracted) indicating the presence of micro-channels throughout the shell. **b**: Magnified image of several channels marked in A and including rulers to measure the inner and outer diameter.

In order to investigate the extent of porosities in the shells in more detail, a series of electron tomography experiments were performed on each MC shell. 3D visualizations of the reconstructions are presented in Figure 6. An orthogonal slice through the 3D reconstruction of MC1X with extracted core is presented in Figure 6a, whereas Figure 6c shows an orthogonal slice for the same type of capsule with the core content (MC1). A similar comparison

is made for MC2X shown in Figure 6e versus MC2 in Figure 6g.

The results demonstrate that there are pores present in the upper halves of the shells of both types of MCs. It is clear that the cases without core extraction (MC1, MC2) show limited penetration of the pores into the shell. On the contrary, the samples with extracted core have porosities extending through the shell, thus forming micro-channels.
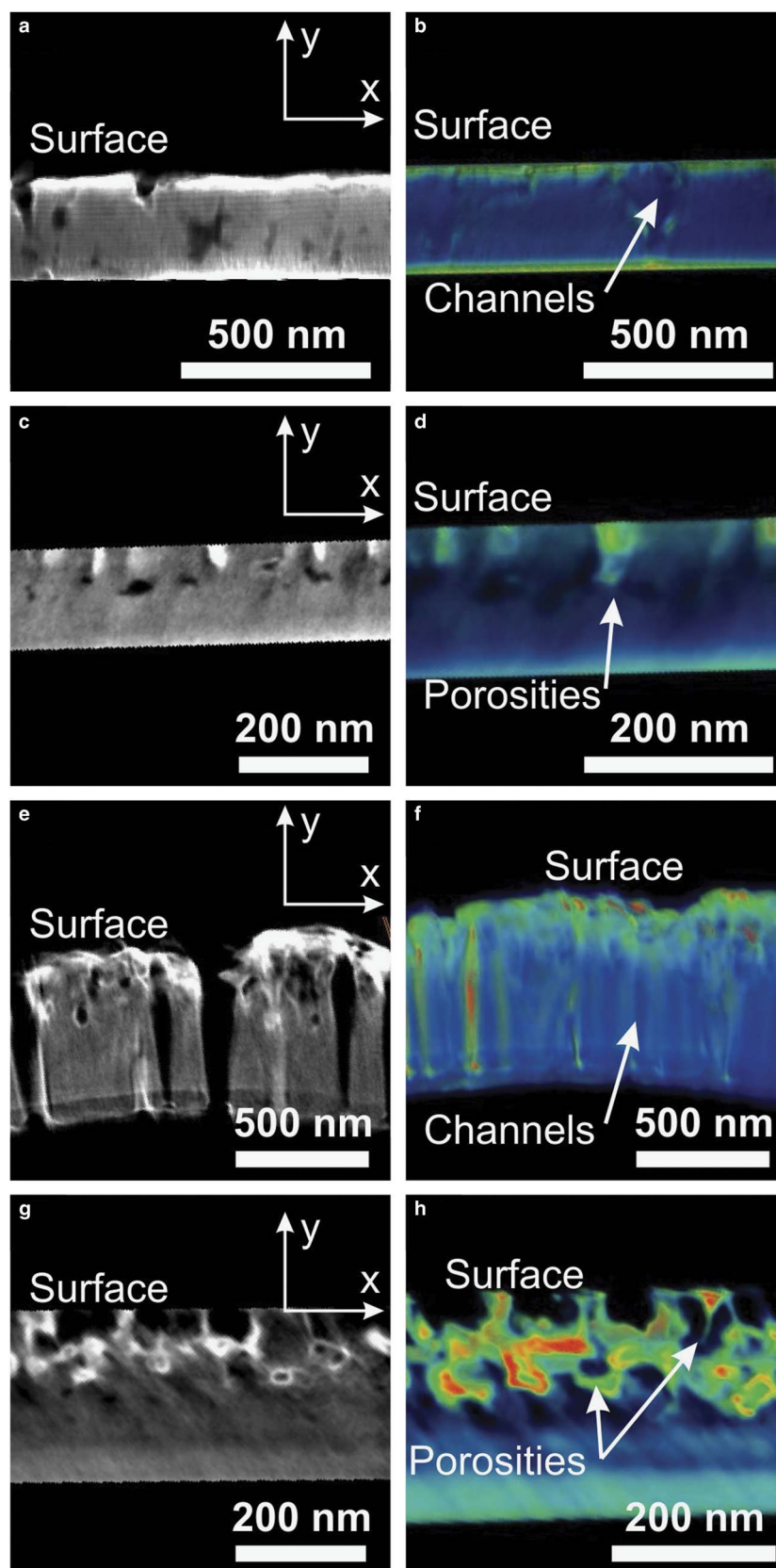
Figure 6. Electron tomography of the microcapsule shells. Left column: XY orthogonal slices through the reconstruction of the capsule shells. Right column: Volume rendering of the 3D reconstruction of microcapsules (Videos are provided in the supporting information). **a,b**: MC1X. **c,d**: MC1. **e,f**: MC2X. **g,h**: MC2.
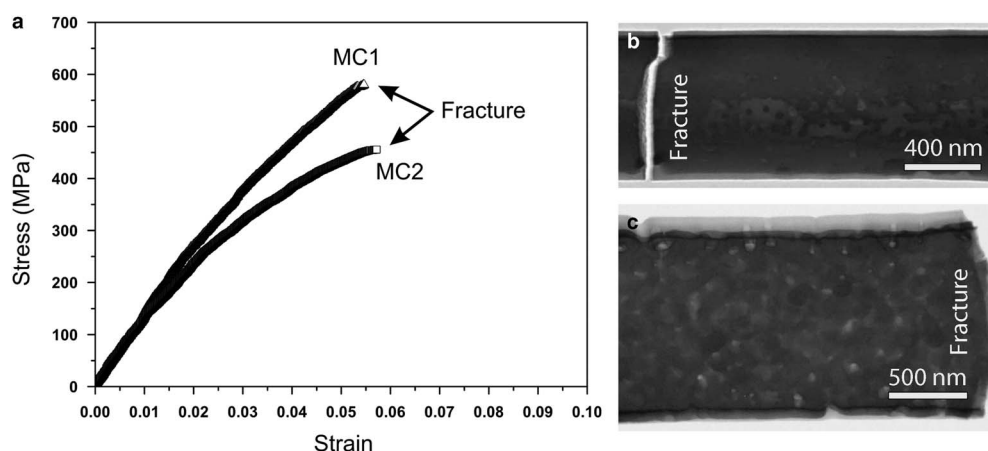
Figure 7. a: True stress-true strain curves obtained in shell samples prepared from microcapsules MC1 and MC2. The samples have been loaded till the fracture point. Note the stiffening size effect in the viscoelastic regime. **b,c**: Snapshot bright-field TEM images obtained after the fracture in samples prepared from MC1 and MC2, respectively.

In other words, although both capsule types exhibit porosity at the outside surface of the shells, the formation of micro-channels should be attributed to the extraction process. In addition, it is observed that the MC2 exhibits a higher quantity of micro-porosities compared with MC1, which is possibly related to the stronger roughness of the surface of these MCs (Figs. 6h versus 6d). The porous nature of the shell explains the observation of finding cyclohexane in the shell, as seen from the Raman mapping. The fact that the Raman sample was pristine, that is, no extraction has taken place and thus pores are only present at the outside half of the shell, implies that the cyclohexane found in the shell (Fig. 4) originates from outside the capsule, possibly from nearby broken capsules in the sample.

Figure 7a exhibits the true stress-true strain curves extracted from the *in situ* TEM tensile testing of the samples prepared from MC1 and MC2. From this, it can be observed that both specimens exhibit a viscoelastic behavior, which is typically found for polymeric materials. Measured yield stress for both MCs is about 145 MPa. The Young's modulus measured in the purely linear elastic regime is 13.2 GPa for both samples, which is almost twice the value of 7.0 GPa reported for bulk MF (Harper, 2000; Lampman, 2003). In the viscoelastic regime, the 476 nm thick sample prepared on MC1 exhibits a higher stiffness in comparison with the 622 nm thick sample from MC2. This points towards a stiffening size effect on the viscoelastic behavior of the MC shell. However, it is worth noting that the higher quantity of pores in MC2 can also affect the stiffness in the same way. Although fracture stress varies from 450 MPa in MC2 to 580 MPa for MC1, that is, 5.4 and 5.7% fracture strain for MC1 and MC2, respectively, a clear size effect on the fracture strain cannot be concluded. However, it is clear that the values of fracture strain reported here are larger than those reported in the literature for bulk MF (~1%) (Lampman, 2003). This can be attributed to the use of very small samples, which places very strong geometrical constraints on the size
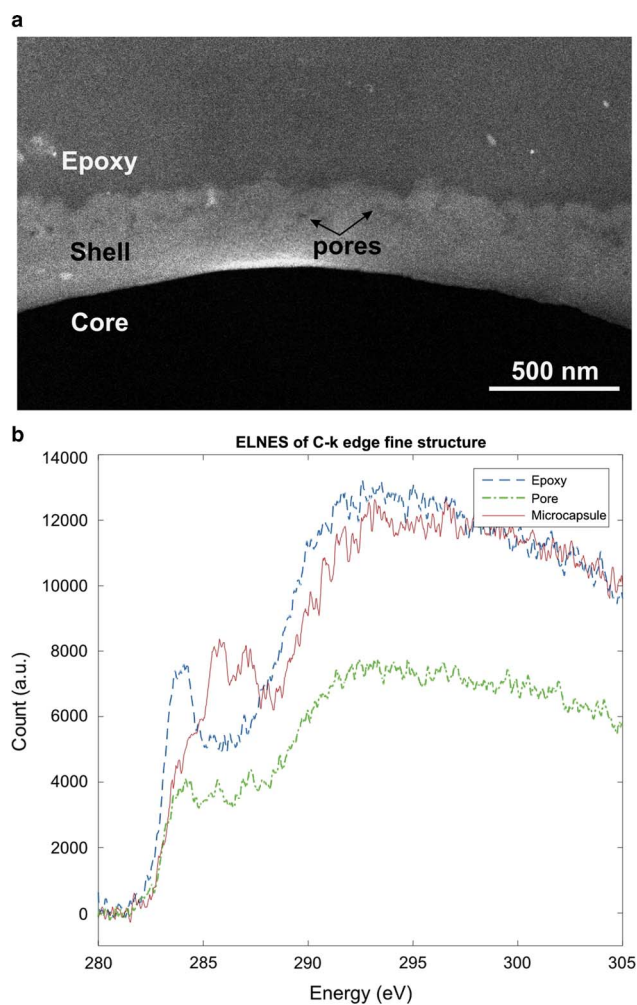

Figure 8. EELS spectra of the microcapsules embedded in epoxy matrix. **a**: High-angle-annular dark-field STEM image of the MC1 shell embedded in the matrix. **b**: Comparison of the characteristic C-K ELNES peaks at different regions in the EEL spectra, revealing the similarity of C bonding in the epoxy and the pores.

of defects that can trigger fracture. In Figures 7b and 7c, it is confirmed that the samples fractured in a brittle manner. Clear changes in the size of the micropores were not observed during the *in situ* TEM straining.

In the structural investigation, it was shown that the surface granulation occurring during the synthesis can be related to the formation of porosities in the outside part of the MC shell. To elucidate the effect of the micropores on the embedding behavior of the MCs, we investigated epoxy embedded MCs using analytical STEM.

Figure 8a shows a cross-section through the MC1 shell after embedding into an epoxy medium with the different regions identified for EELS analysis. It is clear that the shell is well adjoined to the epoxy matrix. To study the possible penetration of the chemicals used for the preparation of the epoxy matrix into the micropores of the capsule shell, spectral imaging using STEM-EELS was performed on a selected region. Subsequently, using the core-loss edges for the C the energy-loss near-edge structure (ELNES) was extracted from the EELS yielding Figure 8b (and N shown in Supplementary File S1). The ELNES signatures of both epoxy matrix and the MC lower half of the shell where no pores are expected, are shown, together with the signatures from the area containing pores. A closer look at the ELNES fine structure of the C-K edge reveals that the curve has mixed characteristics of MC shell and epoxy. This observation suggests that the epoxy compounds may have penetrated in the porous features of the MC shell during the embedding process.

> **Supplementary File S1**
>
> Supplementary File S1 can be found online. Please visit journals.cambridge.org/jid_MAM.

Summary

MCs belong to a large group of advanced materials and have many applications from controlled drug delivery to self-healing composite polymers. Essentially, MCs provide the protection of the core material from the environment and deliver the core material at the targeting point. To understand the mechano-chemical properties of the MCs at sub-micron scale for a given system enables one to tune the structural as well as synthetic parameters for specific applications. SEM investigations have shown that the MF MCs prepared using polycondensation are spherical and exhibit a granulated surface. The grains on the surface of MCs are attributed to formation during synthesis because of precipitation of high molecular weight pre-polymer. Raman spectroscopy imaging reveals that the core content is indeed present in the pristine MCs. Electron tomography reconstructions of the core-extracted compared with non-extracted MCs indicate that porosities at the surface of the capsules, existing in pristine filled MCs, were extended through the shell-forming micro-channels in the extracted ones. *In situ* TEM tensile tests performed on the MC shells indicate a typical viscoelastic behavior for MF. Although the Young's modulus of the MC shells is found to be twice as high compared with reported values for the bulk, the fracture strain is measured to be about 5–6%, which is considerably larger than that of bulk MF. STEM-EELS investigation of epoxy embedded MCs shows that the capsules are well embedded in the epoxy and reveals penetration of epoxy into the pores at the surface of the MC shells.

Acknowledgments

References

Andrade, B., Song, Z., Li, J., Zimmerman, S.C., Cheng, J., Moore, J.S. … Katz, J.S. (2015). New Frontiers for Encapsulation in the Chemical Industry. *ACS Appl Mater Interfaces* **7**(12), 6359–6368.

Blaiszik, B.J., Caruso, M.M., McIlroy, D.A., Moore, J.S., White, S.R. & Sottos, N.R. (2009). Microcapsules filled with reactive solutions for self-healing materials. *Polymer* **50**(4), 990–997.

Deleu, W.P.R., Rivero, G., Teixeira, R.F.A., Prez, F.E.Du & Vos, D.E.De. (2015). Metal—organic frameworks encapsulated in photocleavable capsules for UV-light triggered catalysis. *Chem Mater* **27**(16), 5495–5502.

Devarajan, P.V. & Jain, S. (2014). *Targeted Drug Delivery : Concepts and Design*. Springer, Cham Heidelberg, New York, Dordrecht, London: Springer International Publishing. ISBN:978331 9113555.

Harper, C.A. (2000). *Modern Plastics Handbook*. New York: McGraw-Hill. ISBN:9780070267145.

Hillewaere, X.K.D. & Du Prez, F.E. (2015). Fifteen chemistries for autonomous external self-healing polymers and composites. *Progress in Polymer Science* **49–50**, 121–153.

Hillewaere, X.K.D., Teixeira, R.F.A., Nguyen, L.-T.T., Ramos, J.A., Rahier, H. & Du Prez, F.E. (2014). Autonomous self-healing of epoxy thermosets with thiol-isocyanate chemistry. *Adv Funct Mater* **24**(35), 5575–5583.

Hu, J., Chen, H.-Q. & Zhang, Z. (2009). Mechanical properties of melamine formaldehyde microcapsules for self-healing materials. *Mater Chem Phys* **118**(1), 63–70.

Idrissi, H., Bollinger, C., Boioli, F., Schryvers, D. & Cordier, P. (2016). Low-temperature plasticity of olivine revisited with in situ TEM nanomechanical testing. *Sci Adv* **2**(3), doi:10.1126/sciadv.1501671.

Idrissi, H., Kobler, A., Amin-Ahmadi, B., Coulombier, M., Galceran, M., Raskin, J.-P. & Schryvers, D. (2014). Plasticity mechanisms in ultrafine grained freestanding aluminum thin films revealed by in-situ transmission electron microscopy nanomechanical testing. *Appl Phys Lett* **104**(10), 101903.

JAHROMI, S., LITVINOV, V. & GELADÉ, E. (1999). Physical gelation of melamine formaldehyde resin solutions. II. A combined light-scattering and low-resolution relaxation proton NMR study. *J Polym Sci Part B Polym Phys* **37**(23), 3307–3318.

LAMPMAN, S. (2003). *Characterization and Failure Analysis of Plastics*. Ohio: A S M International. ISBN:9781615030736.

LONG, Y., SONG, K., YORK, D., ZHANG, Z. & PREECE, J.A. (2013). Engineering the mechanical and physical properties of organic-inorganic composite microcapsules. *Colloids Surf A* **433**, 30–36.

NELSON, G. (2002). Application of microencapsulation in textiles. *Int J Pharm* **242**(1–2), 55–62.

NEUBAUER, M.P., POEHLMANN, M. & FERY, A. (2014). Microcapsule mechanics: From stability to function. *Adv Colloid Interface Sci* **207**(1), 65–80.

PRETZL, M., NEUBAUER, M., TEKAAT, M., KUNERT, C., KUTTNER, C., LEON, G. & FERY, A. (2012). Formation and mechanical characterization of aminoplast core/shell microcapsules. *ACS Appl Mater Interfaces* **4**, 2940–2948.

SHAHIDI, F. & HAN, X.Q. (1993). Encapsulation of food ingredients. *Crit Rev Food Sci Nutr* **33**(6), 501–547.

SU, J.F., WANG, X.Y. & DONG, H. (2012). Micromechanical properties of melamine-formaldehyde microcapsules by nanoindentation: Effect of size and shell thickness. *Mater Lett* **89**, 1–4.

SUN, G. & ZHANG, Z. (2001). Mechanical properties of melamine-formaldehyde microcapsules. *J Microencapsul* **18**(5), 593–602.

VAN AARLE, W., PALENSTIJN, W.J., DE BEENHOUWER, J., ALTANTZIS, T., BALS, S., BATENBURG, K.J., & SIJBERS, J. (2015). The ASTRA Toolbox: A platform for advanced algorithm development in electron tomography. *Ultramicroscopy* **157**, 35–47.

YOW, H.N. & ROUTH, A.F. (2006). Formation of liquid core-polymer shell microcapsules. *Soft Matter* **2**, 940–949.

YUAN, Y.C., RONG, M.Z. & ZHANG, M.Q. (2008). Preparation and characterization of microencapsulated polythiol. *Polymer* **49**(10), 2531–2541.